Applied Surface Science 456 (2018) 351–359

Contents lists available at ScienceDirect

Applied Surface Science

journal homepage: www.elsevier.com/locate/apsusc

Full Length Article

Adsorption sensitivity of Fe decorated different graphene supports toward toxic gas molecules (CO and NO)

Zhengyang Gao[a], Yao Sun[a,*], Minghui Li[a], Weijie Yang[a], Xunlei Ding[b,*]

[a] School of Energy and Power Engineering, North China Electric Power University, Baoding 071003, China
[b] School of Mathematics and Physics, North China Electric Power University, Beijing 102206, China

ARTICLE INFO

Keywords:
Fe-decorated graphene
Adsorption characteristics
Steric effect
Fermi softness

ABSTRACT

Sensitivity of Fe-decorated graphene with three different graphene-based supports (single vacancy, double vacancy and four nitrogen decorated) toward toxic gas CO and NO has been investigated by first-principles density functional theory (DFT) calculations. The adsorption configuration, adsorption energy, charge transfer, density of states, competitive behaviors of CO and NO on Fe/GN are thoroughly discussed. Furthermore, Fermi softness is investigated to evaluate the reactivity of the Fe/GN substrates surface. It is found that NO is strongly adsorbed on Fe/GN with considerable adsorption energy of 2.04–2.41 eV, while CO is relatively weaker adsorbed on the same substrates with adsorption energy of 1.10–1.53 eV. Based on our calculation, when CO and NO exist simultaneously, the possibility of adsorption CO can be neglected on the Fe/GN surface. In addition, Fermi softness is a good descriptor to characterize the reactivity of our Fe/GN surface. Our results could provide crucial information for adsorption sensing of NO on Fe/GN, which may be a useful clue for the design and fabrication of Fe-decorated graphene as NO sensors and adsorbent.

1. Introduction

The demand for high sensitivity, high response, high selectivity, high reliability, fast recovery, and low cost miniaturized sensors has prompted scientists to seek new gas sensing systems based on new nanomaterials. Graphene as a two-demensional carbon sheet is an advanced material, its unique long-range π-conjugated structure brings graphene outstanding mechanical and electrical properties [1–4]. Meanwhile, disordered graphene has gained extensive attention. Researchers found several unique aspects of thermal transport in disordered graphene such as milder suppression of thermal conductivity and negligible diffusion contributions [5]. The mild suppression originates from the presence of low-frequency vibrational modes and help to preserve the thermal conductivity in the presence of disorder [6–8]. Decorated with impurities may allow to tune the chemical sensitivity and the properties of graphene [9–11]. Under molecular adsorption, graphene can change its local electronic distributions by charge transfer processes, resulting in high electronic responses due to changes in the electron conductance [12]. Thus, graphene-based materials served as filter membranes [13,14] and chemical sensors [15–18].

Theoretical studies reveal that replacement of atom by doping modifies the band structure of graphene, thus the applications of graphene could be mainly improved. However, metal adatoms on graphene typically have low activation barriers for diffusion and therefore are very mobile at room temperature, which would hinder the performance of the surface [19]. To conquer this puzzle, study showed that the creation of vacancies and filling these vacancies with desired dopants is an efficient way to decorate graphene [20]. In order to embed single metal atom in graphene, Robertson et al. showed that mono and divacancy in graphene within a defined area were created by focused electron beam irradiation [21]. Single vacancy (SV) is formed by removing one C atom, double vacancy (DV) is created by removing two adjacent carbon atoms from graphene surface and previous research demonstrate that the presence of double vacancy defect issues in increasing reactivity and instability of graphene surface [22,23]. To reduce the instability of the DV structure, four nitrogen atoms have been introduced to substitute the dangling bonds in double vacancy area, in addition, the reduction in the amount of free electrons which provides an effective chemical pathway to coordinate graphene electronic properties [24]. Dehui Deng et al. demonstrated that the FeN4 centers have been successfully embedded into the matrix of graphene via high-energy ball milling of FePc and GN composites [25].

The Fe-embedded graphene has shown good activities and thermal stabilities due to the strong bonding between catalyst atoms and the defected graphene substrate [19,25–28]. Considering the practical application, with regards to sensing material selection, single vacancy

* Corresponding authors.
E-mail address: sunnyao07@163.com (Y. Sun).

https://doi.org/10.1016/j.apsusc.2018.06.112
Received 11 February 2018; Received in revised form 6 June 2018; Accepted 13 June 2018
Available online 14 June 2018
0169-4332/

(SV), double vacancy (DV) and four nitrogen atom decorated were selected as three different graphene supports to embed Fe atom. Fe embedded graphene (Fe/GN) meets all requirements to develop low-cost, green and high efficient catalysis. Therefore, Fe/SV, Fe/DV and FeN4/GN act as the detection and sensing material.

The most common source of CO and NO is the exhausts of internal combustion engines [29–32]. CO and NO are highly toxic, colorless, and odorless. At high concentrations, CO and NO can replace oxygen, thereby causing a narotic effect and death by asphyxia [33,34]. In the aspect of electronic structure, different from CO, NO contains a single unpaired electron in the $2\pi^*$ antibonding orbital conferring it a free radical character and making it chemically very reactive [35]. The electron pairing upon adsorption will introduce additional stability and distortion to the coordination around the embedded Fe atom.

Although many efforts have been made to use catalysts to reduce the amount of carbon or nitrogen oxides in the air [36–38], an efficient method of sensing and removing the pollutants is still required. However, only limited studies reported whether Fe/GN is suitable for the detection and sensing of NO [39]. Taking into account the rise of embedded-graphene in adsorption and sensing applications, we theoretically explore the implementation of Fe/GN in the adsorption and subsequent sensing of CO and NO. Firstly, The Fe/GN-adsorbate systems were fully characterized from its geometrical, energetic, electronic and binding properties by means of dispersion corrected DFT simulations. Secondly, in order to illustrate the adsorption difference we discuss the competitive behaviors between the adsorbed CO and NO molecules on substrates. Finally, in order to enhance the comprehending of the difference of adsorption activity, Fermi softness of Fe/GN catalysts has been evaluated. Our investigation could provide a new insight for how Fe/GN substrates could be applied to design more sensitive gas sensing devices.

2. Computational methods

All calculations were performed with the plane-wave DFT method as implemented in the Vienna ab initio simulation package (VASP) [40]. The projector-augmented wave (PAW) method was used to describe the core and valence electrons [41]. The Perdew–Burke–Ernzerhof (PBE) form of the generalized-gradient approximation was employed to describe electron exchange and correlation [42]. All calculations were performed on a 4 × 4 graphene supercell with periodic boundary conditions; periodic images were separated by vacuum in excess of 15 Å to the sheets to prevent spurious image interactions [14].

A kinetic energy cutoff of 500 eV was set in all structural relaxation simulations of CO and NO adsorption and the convergence criterion for the electronic self-consistent iteration is set to 10^{-5} eV. A gamma centered 7 × 7 × 1 k-point mesh was used for the Brillouin zone integration and a gamma centered 15 × 15 × 1 was used for the final density of states (DOS) calculations. In all cases, structural relaxations were performed using a conjugate gradient algorithm until forces on all atoms were below 0.02 eV/Å. All calculations were performed with spin polarization.

In order to verify the steric effect on the adsorption height from gases to Fe, We have chosen $C_{48}H_{18}$ (4 × 4) to represent the graphene to perform a Reduced Density Gradient (RDG) analysis on steric effect [43]. $C_{48}H_{18}$ is so-called coronene-like and was proved to be the smallest molecule that perfectly resembles graphene properties [44–46]. This model could deal with the subject of steric effect conveniently and it has been widely used for the study of similar systems. The ends of all studied models were passivated with hydrogen atoms to avoid the dangling [47]. BLYP-D3 is used with def2-SVP basis sets, and meantime, geometrical Counterpoise Correction (gCP) method is used to account for Basis Set Superposition Error (BSSE) problem. We used RDG graphs to display steric effect [48] which were rendered by Visual Molecular Dynamics (VMD) [49].

Table 1
The binding energy, structural parameters of Fe atom deposition on different supports and the number of transferred charge from metal atom to graphene to different graphene supports.

supports	E_b (eV)[a]	q(|e|)[b]	$d_{Fe\text{-}C/N}$ (Å)[c]	h (Å)[d]
Fe/SV	7.14(7.30[58])	0.69(0.36[24])	1.76(1.77[25])	1.29(1.45[25])
Fe/DV	6.12(6.30[58])	0.90(1.33[59])	1.96(1.97[25])	0.65(0.57[25])
FeN4/GN	7.14(7.07[60])	1.08(1.36[61])	1.90(1.88[62])	0.04(0.03[63])

[a] The binding energy of Fe atom onto graphene, calculated from Eq. (1).
[b] After geometry optimization, the charge of Fe atom transfers to graphene surface (q, in |e|).
[c] The average Fe-C distance in the most plausible adsorption configuration as indicated.
[d] The adsorption height from Fe to the different supports plane.

Throughout this paper, the binding energy (E_b) between Fe adatom and supports and the adsorption energy (E_{ads}) of adsorbate gas on graphene-supported and are obtained from Eqs. (1) and (2) respectively.

$$E_b = E_{sub} + E_{Fe} - E_{sub-Fe} \quad (1)$$

$$E_{ads} = E_{Fe/GN} + E_{gas} - E_{Fe/GN-gas} \quad (2)$$

where $E_{Fe/GN\text{-}gas}$, $E_{Fe/GN}$, E_{gas}, $E_{sub\text{-}Fe}$, E_{Fe} and E_{sub} are the total energy of the given system, the energy of graphene supports, the energy of CO and NO, the total energy of Fe/GN system, the energy of Fe atom, and the energy of graphene supports.

As defined here, more positive values of E_{ads} signify stronger binding. Atomic charges and electrons transfer are evaluated based on the Bader charge analysis [50].

3. Results and discussion

3.1. The most stable geometries for Fe/SV, Fe/DV and FeN4/GN

The most stable configuration of Fe/GN are investigated, and the corresponding energetic and geometrical data are shown in Table 1. The calculated E_b are 7.14, 6.12 and 7.14 eV, respectively. As shown in Fig. 1, the Fe atom stands out of the basal plane of graphene. Our results agree well with previous calculations [19,39,51–55]. The calculated results by ORCA are displayed in Fig. 2. The parameters of optimized structures by ORCA (see Table 2) are similar to that by VASP, therefore the structures are credible.

Bader charge analysis indicates that the Fe atom acts an electron donating support. The transferring electrons (0.69 e) move from the Fe atom to the single vacancy graphene sheet and forms the strong covalent bond between the Fe atom and C atoms. Because the preferential electron accumulation sites are mainly located within the bond rather than heavily centered on a particular atom (see Fig. 5g) [21,56]. Compared with the case of Fe/SV system, the doped Fe atom provides more transferred electrons (0.90 e) to double vacancy graphene system, while the Fe atom transfers the most electrons (1.08 e) to the N4/GN, meanwhile the out-of-plane displacement (h, Table 1) is decreasing from 1.29 to 0.04 Å. In addition, this can suggest that the Fe atom is activated to be more electrophilic by its support.

3.2. CO and NO molecules adsorption on Fe decorated graphene supports

Based on the stable structure of the Fe-graphene substrates, we examine the possible adsorption sites in order to find out the energetically favorable configurations for adsorbates on Fe/SV, Fe/DV and FeN4/GN substrate. The corresponding adsorption energies and structural parameters for the optimized structures are listed in Table 3.

From Fig. 3, just like we see, the larger the volume around the iron atom, the stronger the steric effect, so we can conclude that the steric

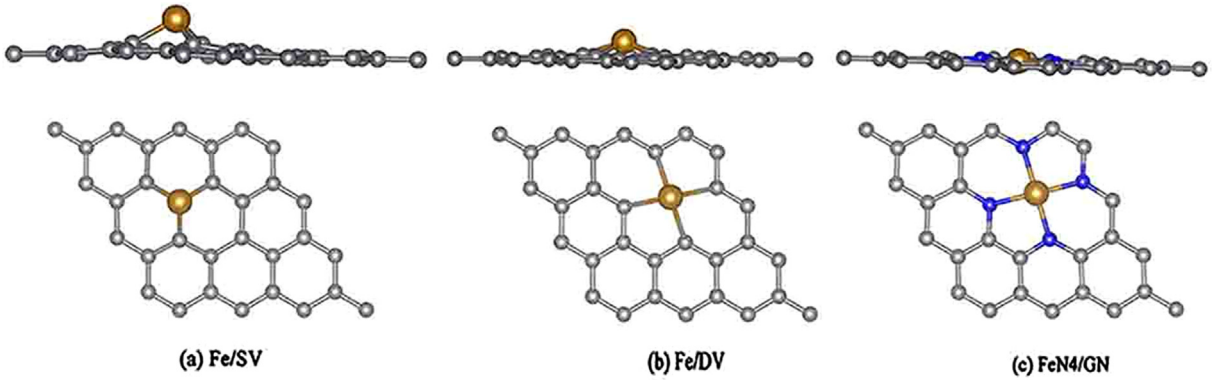

Fig. 1. The side view and top view of the optimized structure of Fe atom embedded in graphene. (a) Fe/SV, (b) Fe/DV and (c) FeN4/GN. Gray, gold and silver balls represent the C, Fe and N atom, respectively. (For interpretation of the references to colour in this figure legend, the reader is referred to the web version of this article.)

hindrance of these three structures are in order: Fe/DV > FeN4/GN > FeSV. Table 3 shows that the distance from Fe atom to C atom (of CO molecule) are in order: Fe/DV > FeN4/GN > FeSV, we consider that the visible differences of adsorption distance are caused by steric hindrance, but the order of adsorption distance of NO is completely opposite and the adsorption distance of NO is little difference. The reason can lie in the extra electron possessed by NO than CO. The three adsorbents are positively charged and the attraction of positive and negative charges overcomes steric hindrance.

Our computed results demonstrate that both CO and NO can adsorb on Fe/GN, the latter has a much stronger adsorption than the former. The individual gas molecule has large energy difference on Fe/GN sheets. The adsorption CO has similar configurations on the different substrates, it prefers to form Fe—C bond which is vertical to the Fe/GN surface with C (CO) atoms bonding to a metal atom and O atoms pointing away the surface, as shown in Fig. 4. As it is clear, six stable structures are estimated for CO and NO over Fe/GN (complexes a, b, c, d, e, f). The computed CO adsorption energy is −1.45, −1.10 and −1.53 eV for Fe/SV, Fe/DV and FeN4/GN, respectively. CO adsorption on FeN4/GN is strongest among these three adsorbent. As for NO, it has relatively larger E_{ads} of −2.24, −2.41 and −2.04 eV, respectively. The adsorption energy of CO and NO adsorption on pristine graphene is 0.05 and 0.30 eV [57,58], therefore, decoration of Fe in graphene significantly enhances the interaction between them, but without being a noble metal, insted being low cost. The most stable configuration is N atom (NO) directly bonded to the Fe atom. In both structures, the NO molecule is tilted with respect to substrates plane. The Fe—N—O bond angle for the most plausible configuration is 159.43° [24], 166.82° and 147.86° on Fe/SV, Fe/DV and FeN4/GN, respectively. The value of bond angle is close to ~145° which is predicted by the Enemark-Feltham formula for $n = 7$. This formula is applied to predict the M—N—O bond angles in metal nitrosyl complexes with $\{M(NO)_x\}^n$ general formula, therein x represents the amount of NO ligands and n denotes total electrons in the metal d orbitals. Based on this formalism, M—N—O angles of ~180° for $n \leq 6$, ~145° for $n = 7$, and ~120° for $n = 8$ have been predicted [59]. To further understand the origin of the differences in electronic structure properties according to the type of adsorbates, we investigate the electron density difference and Bader charge analysis of gases adsorption on Fe/GN substrates. The most favorable configurations along with their electron density difference (EDD) maps are shown in Fig. 5.

Table 2
The comparision of parameters calculated by VASP and ORCA.

supports	$d_{Fe\text{-}C/N}$(Å)[a]/VASP	$d_{Fe\text{-}C/N}$(Å)[b]/ORCA	h(Å)[c]/VASP	h(Å)[d]/ORCA
Fe/SV	1.76	1.79	1.29	1.20
Fe/DV	1.96	1.96	0.65	0.65
FeN4/GN	1.90	1.92	0.04	0.01

[a] The average Fe-C/N distance in the most plausible configuration calculated by VASP.
[b] The average Fe-C/N distance in the most plausible configuration calculated by ORCA.
[c] The adsorption height from Fe to the different supports plane calculated by VASP.
[d] The adsorption height from Fe to the different supports plane calculated by ORCA.

Fe atoms along with CO molecule form a similar carbonyl compounds, thereinto, the HOMO orbital containing electrons participate in the formation of σ bond while the empty π orbital namely LUMO involves in the formation of π bond. According to Bader charge analysis, CO gains 0.13–0.15e to the $2\pi^*$ orbitals. The electron configuration of

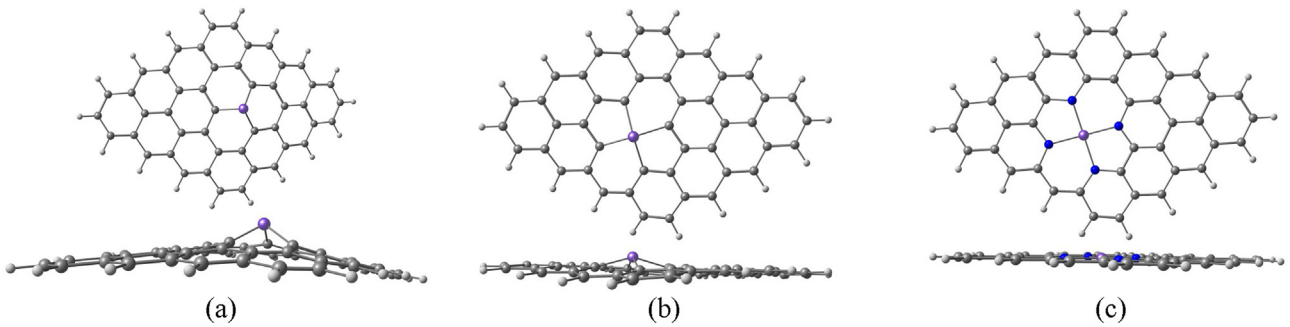

Fig. 2. The side view and top vies of the optimized structure of Fe atom embedded in $C_{48}H_{18}$ (4*4). (a) Fe/SV, (b) Fe/DV and (c) FeN4/GN. Gray, purple and blue balls represent the C, Fe and N atom, respectively. (For interpretation of the references to colour in this figure legend, the reader is referred to the web version of this article.)

Table 3
The structural and energetic parameters for CO and NO adsorption on Fe/GN composites.

supports	E_{ads}/eV[a]		$d_{C-O/N-O}$/Å[b]		$d_{Fe-C/Fe-N}$/Å[c]		$\Delta h_{Fe-plane}$/(Å)[d]		$\Delta q_{Fe\ and\ CO}$/e[e]		$\Delta q_{Fe\ and\ NO}$/e[e]	
	CO	NO	CO	NO	CO	NO	CO	NO	Fe	CO	Fe	NO
Fe/SV	−1.45	−2.24	1.16	1.19	1.16	1.71	0.04	0.16	−0.05	0.13	−0.17	0.32
Fe/DV	−1.10	−2.41	1.16	1.19	1.85	1.66	0.02	0.03	−0.05	0.14	−0.01	0.27
FeN4/GN	−1.53	−2.04	1.17	1.19	1.71	1.69	0.30	0.44	0.13	0.15	−0.03	0.30

[a] Adsorption energy (E_{ads}) of adsorbates on the different supports calculated from Eq. (2).
[b] Structural parameters for the CO and NO in the most plausible adsorption configuration.
[c] The nearest distance ($d_{Fe-CO/NO}$) between the adsorbate and Fe atom.
[d] The distance changes from Fe to graphene plane after adsorption.
[e] Electron transfer (Δq) from the Fe atom to the adsorbates ("+" represents accumulation;"−" represents depletion.

CO is $[1\sigma^2 2\sigma^2 3\sigma^2 4\sigma^2 1\pi^4 5\sigma^2 2\pi]$, so, the empty anti-bonding orbital of CO is occupied with the transferred electrons which slightly weaken the C—O bond from 1.13 Å in the free CO/NO molecule to 1.16–1.17 Å in the adsorbed configuration. Herein, the NO molecule adsorbs stronger than CO on the same substrates, and a larger amount of electrons 0.27–0.32e transfers from the Fe/GN to the partly filled $2\pi^*$ orbitals of NO (the electron configuration is $[1\sigma^2 2\sigma^2 3\sigma^2 4\sigma^2 1\pi^4 5\sigma^2 2\pi^1]$. The N—O bond length is slightly elongated from 1.15 Å in free NO to 1.19 Å. The Pauling eletronegativity of Fe, N and O atom is 1.83, 3.04 and 3.44, respectively [39]. Electronegativity is chemical property that describes the tendency of an atom or a functional group to attract electrons towards itself. Therefore, Fe/GN sheet lose electrons to NO. In addition, this behavior is consistent with these papers [60,61]. Such a large electron transfer is expected to induce sizeable changes on the conductivity of the system [18].

The electron density difference (EDD, Fig. 5) is calculated from the difference of the electron densities between the whole structure and its two isolated parts, which are the CO/NO and the Fe/GN. The charge depletion and accumulation sites are displayed in cyan and yellow. The definition: $\Delta\rho = \rho_{gas\text{-}Fe/GN} - \rho_{gas} - \rho_{Fe/GN}$ is considered and implied to both resonance character and the transfer of an electron between fragments in the system after binding. The EDD plot shows the charge transfer from Fe/GN to gas and also the reduction of the C═O and N═O bond. In Fig. 5f, the N4/GN sheet shows a nonnegligible electron density depletion, this result indicates that the electron density on the graphene sheet can transfer to the gas molecule, where Fe atom serves as an electron transfer carrier. The EDD plot agrees well with the results of the Bader charge analysis. The corresponding EDD map also shows a significant electron density rearrangement upon the complex formation. In the six sectional views, there are overlaps of the yellow region between C atom of the CO molecule and N atom of the NO molecule and Fe atom, which indicates the strong binding of C/N atom to the Fe atom. This shows that the six kind of adsorption configurations are referred to its chemical characteristic [62].

3.3. Thermodynamic corrections and competitive behaviors

In associated with the practical application, thermodynamic corrections and Boltzmann distribution can help understand the adsorption probability of CO and NO molecules on Fe/GN. The standard conditions (295.15 K, 1 bar) are employed in the present work. The Gibbs energy of substrates and gas are calculated from the following formula [63]:

$$G_{gas} = E_{ele} + ZPE + RT - TS \quad (3)$$

$$G_{solid} = E_{ele} + ZPE - TS \quad (4)$$

$$\Delta G_{ads} = G_{Fe/GN} + G_{gas} - G_{Fe/GN-gas} \quad (5)$$

where E_{ele} is the ground-state energy of the system, ZPE is the zero correction energy, R is gas constant, T is the temperature, S is the entropy of the system, G_i is the Gibbs free energy of gas, adsorbed system and clean surfaces and ΔG_{ads} is the Gibbs free adsorption energy , respectively. The vibrational contributions to zero-point energy corrections and to the entropy are systematically calculated and included in all models.

The computed CO/NO adsorption energy is 1.96/2.52, 1.66/2.77 and 1.94/2.43 eV for Fe/SV, Fe/DV and FeN4/GN, respectively. The competition behaviors between the adsorbed CO and NO molecules on Fe/GN are considered according to Boltzmann distribution $\left(\frac{N(NO)}{N(CO)} = \exp\left(-\frac{E(NO)-E(CO)}{kT}\right)\right)$ under standard conditions. The adsorption probability of NO is 3.95×10^9, 5.05×10^{18}, and 1.82×10^8 times higher than CO on Fe/SV, Fe/DV and FeN4/GN, respectively. Hence, the Fe/GN substrate exhibits the high sensing performance for NO gases. Based on the analyses, under standard conditions, only NO adsorbed on Fe/GN with CO free, the possibility of adsorption CO can be neglected on the Fe/GN surface. Due to the excellent performance of these substrates on adsorbing NO, these three substrates could be used to capture NO. Among these, Fe/DV is the most optimal selection.

3.4. The effect of NO adsorption on electric conductivity

The energy of Fermi level, the conduction band minimum (CBM),

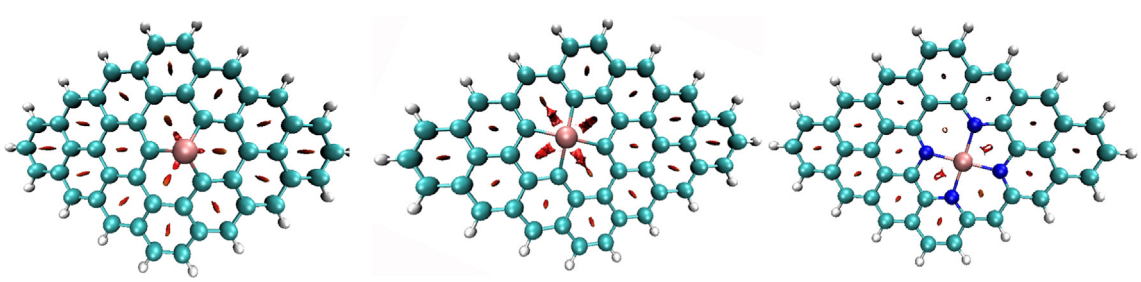

Fig. 3. The RDG graph drew by Multiwfn. The watermelon red represents the steric hindrance. From left to right in order, take the following measures: Fe/SV, Fe/DV and FeN4/GN respectively.

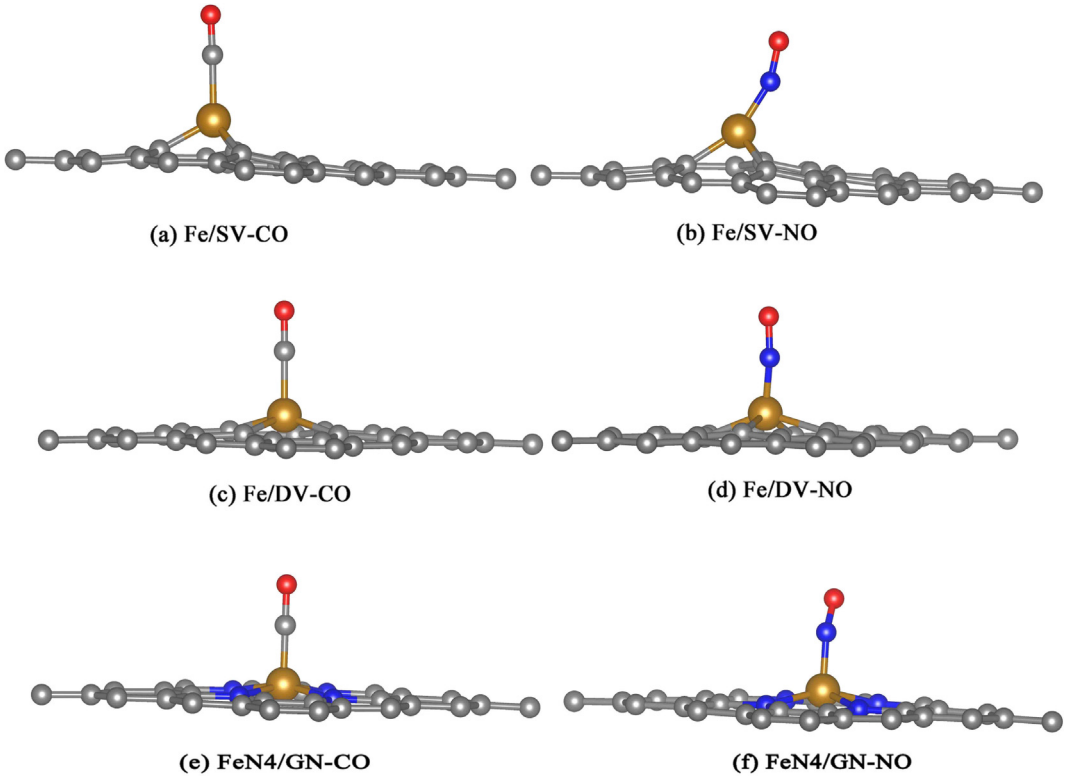

Fig. 4. Optimized structures of CO and NO molecules over Fe/GN.

the valence band maximum (VBM), band gap (E_g) were calculated and are provided in Table 4. It is also obvious from Table 4 that after gas adsorption on substrates, there is apparent shift in either the VBM, CBM, E_F or E_g compared to the isolated Fe/GN, providing that there was hybridization which corresponds to strong interaction. Upon adsorption of CO and NO on Fe/GN, the VBM and CBM slightly shifts on the

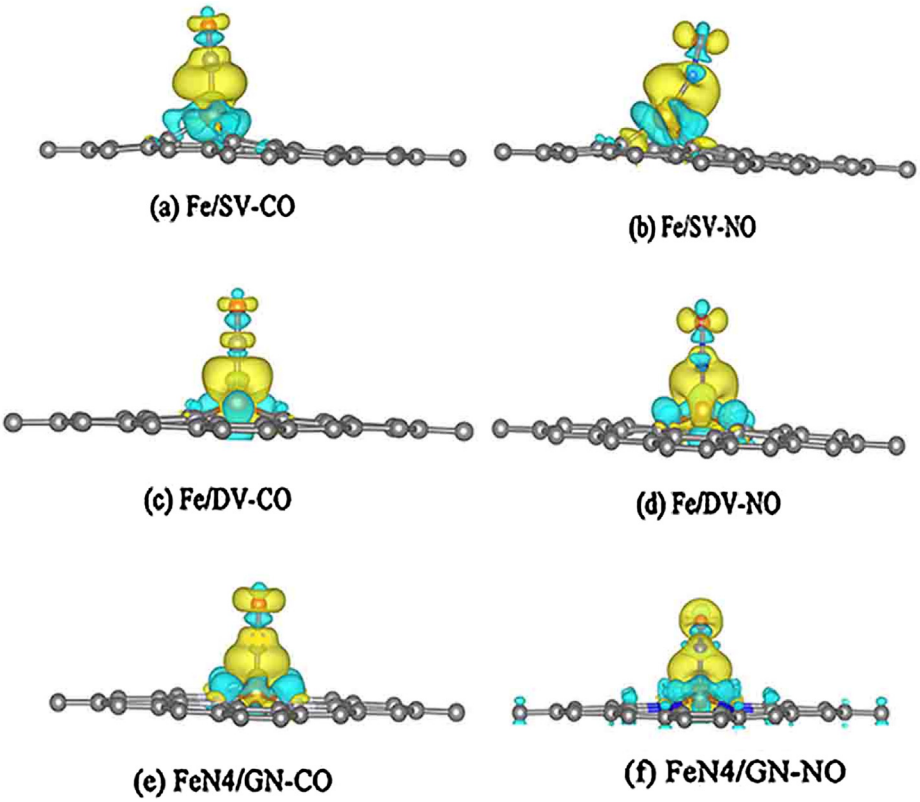

Fig. 5. Corresponding electron density difference (EDD) maps (0.001 au), the yellow and cyan colors denote the electron density accumulation and depletion regions, respectively. (For interpretation of the references to colour in this figure legend, the reader is referred to the web version of this article.)

Table 4
Adsorption energy (E_{ads}) and orbital characteristic:VBM, CBM, energy of Fermi level (E_{FL}), CBM - VBM energy gap (E_g) for all complex and non-complex forms of Fe/GN.

system	E_F/eV	VBM/eV	CBM/eV	E_g/eV
CO	−8.981	−9.028	−2.137	6.890
NO	−4.609	−4.609	−0.225	4.383
Fe/SV	−2.104	−2.316	−1.869	0.447
CO-Fe/SV	−1.947	−2.156	−1.737	0.418
NO-Fe/SV	−2.493	−2.412	−2.404	0.007
Fe/DV	−2.548	−2.466	−2.455	0.010
CO-Fe/DV	−2.747	−2.666	−2.647	0.018
NO-Fe/DV	−2.871	−2.789	−2.780	0.008
FeN4/GN	−1.967	−1.916	−1.824	0.092
CO-FeN4/GN	−2.167	−2.255	−2.069	0.186
NO-FeN4/GN	−2.025	−1.946	−1.873	0.072

adsorbate for all adsorption configuration expect for the adsorption of CO on Fe/SV. After CO and NO adsorption, there are few changes of the overall E_g. For Fe/DV and FeN4/GN, the E_g of CO adsorption slightly increases while the E_g of NO adsorption reduces a little. It's rather special for Fe/SV that the E_g of CO adsorption slightly decreases while the E_g of NO adsorption significantly degenerate. The larger E_g indicates that the adsorption of gas reduces the electric conductivity of the substrates. It is well known that E_g is a crucial factor determining the electrical conductivity of a material and there is a classic criterion between them as follows: $\sigma \propto \exp(\frac{-Eg}{2kT})$ [64], where σ is the electric conductivity of semiconductor and k is the Boltzmann's constant. It's determined that at a fixed temperature, even if the change of E_g is little, due to the conductivity exponentially correlated with negative value of E_g, the electric conductivity of conducting material would undergo considerable changes. However, ascribing the change in electrical conductivity solely to the change in band gap Eg is far from being sufficient. Electrical conductivity of graphene was investigated by many authors and the current–current correlation function in the random phase approximation are the Kubo response formalism and Boltzmann transport equation. It's sensitive to mass-gap parameter, chemical potential, scattering rate, energy dispersion, carrier density, temperature, etc [65,66]. Based on the above analysis, it is expected that Fe/GN could directly convert the presence of NO to the electrical signal.

3.5. Electronic properties:density of states and Fermi softness

To get more insights into the adsorption of CO and NO onto Fe/GN, relevant electronic properties are analyzed on: density of states (DOS) and Fermi softness.

3.5.1. Density of states of CO and NO adsorbed Fe embedded graphene

To figure out the effect of the Fe/GN toward CO and NO molecule, the projected density of states (PDOS) of Fe/GN with CO and NO adsorption were calculated. Fig. 6 clearly shows that there is a strong hybridization between the Fe-d orbitals an NO orbitals. Especially, the $2\pi^*$ orbital of the CO and NO molecule is dominantly occupied. This confirms that Fe/GN can activate an CO and NO molecule and facilitate further reactions. But, there is no obvious hybridized states between Fe-d orbitals and the CO orbitals. In Fig. 6, the occupied molecular orbitals of gas move away from the Fermi energy level with orbital energies reduction making adsorbed gas stable.

Diatomic molecules CO adsorbate systems with no unpaired electrons but with an unsaturated π-electron system, the bonding of CO to Fe atom is through a FMO theory where a dative bond between the 5σ lone-pair electrons and Fe'3d orbital is formed, leading to charge donation into the Fe atom which is compensated by back-donation into the molecular $2\pi^*$ orbital. It should be noted that the internal molecular bond is weakened due to the increased population of the antibonding $2\pi^*$ in the back-donation, which is consistent with what we discussed earlier. For NO with one additional π-electron, the π-interaction is enhanced while the σ-interaction remains quite similar to that of CO leading to lager probability for adsorption in sites with higher coordination. The NO bonding to surfaces where the adsorbate has unpaired electrons available for covalent interaction with unsaturated electronic states on the metal surface and forms electron pairs with the metal atoms at the surface.

3.5.2. Fermi softness

Researchers lucubrate the material structure and chemical reaction laws applying the frontier molecular orbital theory, however, the frontier molecular orbital theory can't be applied to solid surface studies because the amount of atoms in the solid is large and the surface bonding is complex. Recently, Zhuanglin'team presented a new descriptor that characterizes the solid surface frontier orbital, making it possible to describe the description of solid surface reactivity intuitively and quantitatively.

Zhuang Lin et al. proposed that the contribution of each energy level in the energy band to the reactivity is described by a weight function. The maximum value appears at the Fermi level and gradually decreases with the energy change to zero, and the physical quantity obtained by weighting the energy density is defined as Fermi softness. Studies have shown that Fermi softness not only has a good correlation with the adsorption energy, but also provides an atomic scale surface reactive spatial image. The method successfully reveals the fine reactive structure of many complex catalyst surfaces and the spatial anisotropic catalytic properties of the chemical reaction. At present, none of theoretical methods can realize the unique funcitons. However, there are scarce reports about this conception applied to single atom catalysts. Hence, we apply the concept of Fermi softness to our adsorbent-adsorbate systems.

Fermi softness are measured via the following definitions:

$$S_F = \int g(E)w(E)dE = -\int g(E)f'_T(E-E_F)$$

$$-f'_T(E-E_F) = \frac{1}{kT}\cdot\frac{1}{(e^{(E-E_F)/kT}+1)(e^{(E_F-E)/kT}+1)}$$

where g(E) is the density of states, w(E) derives from the Fermi-Dirac distribution, *kT* is the nominal electron temperature (k is Boltzmann's constant, T is the parametric temperature).

We also calculated the correlation coefficient between Fermi Softness and the adsorption energy, and plotted with *kT* and the correlation coefficient R^2. From Fig. 7, it can be seen that the trend of the two gases is roughly the same, and all of them are presented as an open parabolic shape. We also calculated the Fermi softness of different substrates under different *kT*. The Fermi softness of Fe/SV and FeN4/GN showed a clear upward trend in the *kT* range of 0.1–0.25 eV, and then the Fermi softness of Fe/SV decreases slowly while the Fermi softness of FeN4/GN increases slowly; The Fermi softness of Fe/DV varies little over the entire *kT* range.

The correlation coefficient between Fermi softness and adsorption energy is also considered, by adjusting the nominal electronic temperature, the S_F exhibits a significant correlation with the surface reactivity. As Fig. 7 illustrated, the two trend presented as an open parabolic shape.

The adsorption of NO can correlate highly with the S_F of three substrates when $kT = 0.15$ eV, while the highest correlation occurs at $kT = 0.45$ eV for the adsorption of CO, which illustrates that the Fermi softness can be used as a new descriptor to characterize the reactivity of our Fe/GN system.

4. Conclusion

To summary, using the first principles calculations, we explored the plausible configuration of CO and NO adsorption on the Fe/GN,

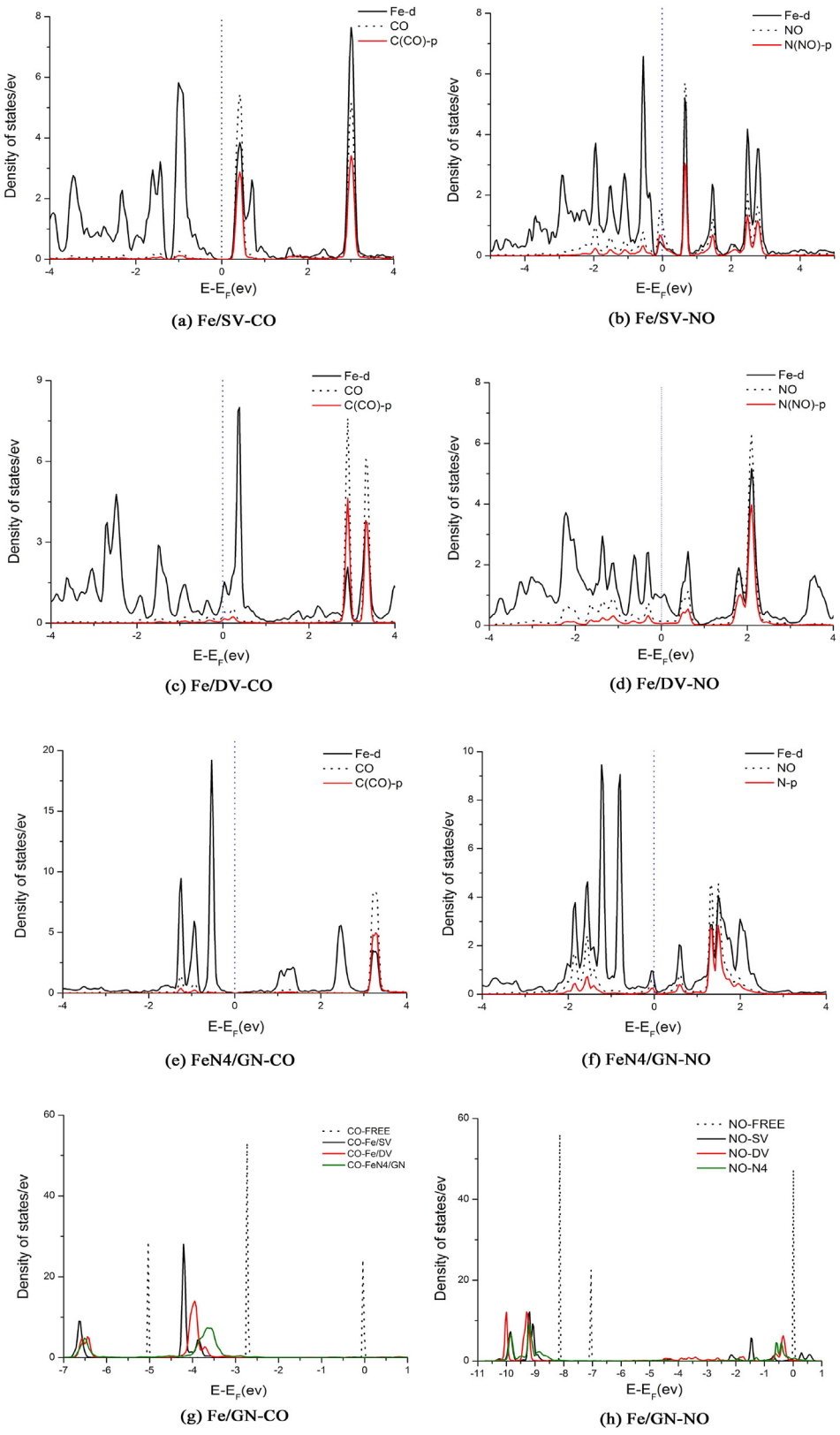

Fig. 6. The PDOS profiles of gas adsorbed Fe/GN. In Fig. 3a–f, the black and red solid line denoted the Fe'3d orbitals and C or N atom'2p orbitals from gas, respectively. The black dotted lines denoted the DOS of adsorbed gas molecule. The Fermi energy level is plotted in blue dotted line. (For interpretation of the references to colour in this figure legend, the reader is referred to the web version of this article.)

rationalized the possibility of Fe/GN as a potential gas sensing device for detecting NO and mainly focused on how electronic properties of Fe decorated with different graphene supports affect the CO and NO adsorption. Compared with the Fe/SV and FeN4/GN, the Fe/DV exhibits the high sensing performance for the adsorbed NO meanwhile avoids the poisoning of CO. Based on analysis, Fermi softness was an

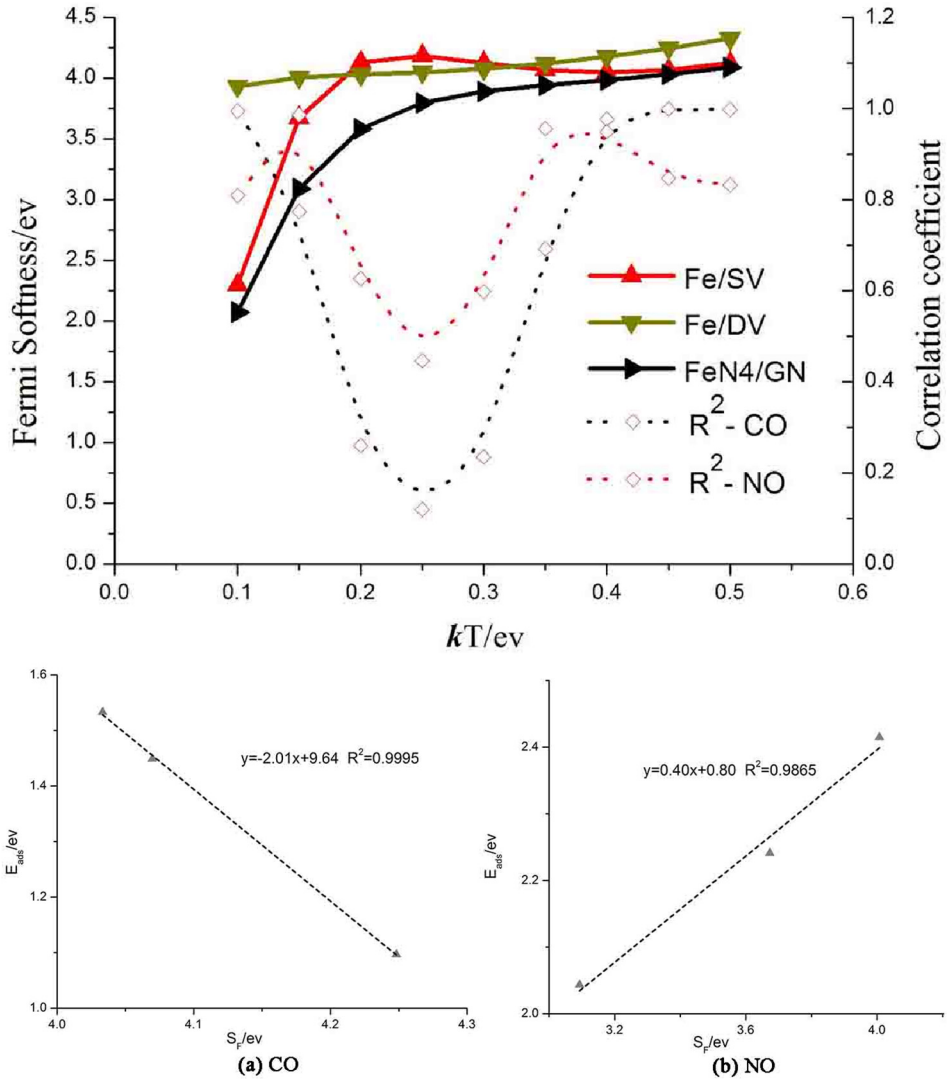

Fig. 7. The correlation coefficient between Fermi softness and adsorption energy and Fermi softness changes with kT.

effective descriptor of reactivity of the Fe/GN substrates surface. We hope that this work will cast insight into the targeted design of effective Fe/GN for NO adsorption, detection and sensing device.

Acknowledgement

This work was supported by the National Natural Science Foundation of China (No. 91545122) and Beijing Natural Science Foundation (2182066).

References

[1] A.K. Geim, Graphene: status and prospects, Science 324 (2009) 1530.
[2] C. Lee, X. Wei, J.W. Kysar, J. Hone, Measurement of the elastic properties and intrinsic strength of monolayer graphene, Science 321 (2008) 385.
[3] A.A. Balandin, S. Ghosh, W. Bao, I. Calizo, D. Teweldebrhan, F. Miao, C.N. Lau, Superior thermal conductivity of single-layer graphene, Nano Lett. 8 (2008) 902.
[4] N.M.R. Peres, The electronic properties of graphene and its bilayer, Vacuum 83 (2009) 1248–1252.
[5] T. Zhu, E. Ertekin, A generalized Debye-Peierls/Allen-Feldman model for the lattice thermal conductivity of low dimensional and disordered materials, Phys. Rev. B 93 (2016).
[6] T. Zhu, E. Ertekin, Phonons, localization, and thermal conductivity of diamond nanothreads and amorphous graphene, Nano Lett. 16 (2016) 4763–4772.
[7] T. Zhu, E. Ertekin, Phonon transport on two-dimensional graphene/boron nitride superlattices, Phys. Rev. B 90 (2014).
[8] C. Xiao, Z. Li, K. Li, P. Huang, Y. Xie, Decoupling interrelated parameters for designing high performance thermoelectric materials, Accounts. Chem. Res. 47 (2014) 1287.
[9] G. Wu, K.L. More, P. Xu, H.L. Wang, M. Ferrandon, A.J. Kropf, D.J. Myers, S. Ma, C.M. Johnston, P. Zelenay, A carbon-nanotube-supported graphene-rich non-precious metal oxygen reduction catalyst with enhanced performance durability, Chem. Commun. 49 (2013) 3291–3293.
[10] E. Antolini, Graphene as a new carbon support for low-temperature fuel cell catalysts, Appl. Catal. B Environ 123–124 (2012) 123–124.
[11] A. Tiwari, Graphene-based composite materials, Dissertations Theses - Gradworks 442 (2015) 282–286.
[12] L. Kong, A. Enders, T.S. Rahman, P.A. Dowben, Molecular adsorption on graphene, J. Phys. Condens. Matter 26 (2014) 443001.
[13] D.J.D. Durbin, C. Malardierjugroot, Density functional theory analysis of metal/graphene systems as a filter membrane to prevent co poisoning in hydrogen fuel cells, J. Phys. Chem. C 115 (2011) 808–815.
[14] L. Wang, Q. Luo, W. Zhang, J. Yang, Transition metal atom embedded graphene for capturing CO: A first-principles study, Int. J. Hydrogen Energ. 39 (2014) 20190–20196.
[15] H.J. Yoon, D.H. Jun, J.H. Yang, Z. Zhou, S.S. Yang, M.C. Cheng, Carbon dioxide gas sensor using a graphene sheet, Sens. Actuators, B 157 (2011) 310–313.
[16] Y.H. Zhang, Y.B. Chen, K.G. Zhou, C.H. Liu, J. Zeng, H.L. Zhang, Y. Peng, Improving gas sensing properties of graphene by introducing dopants and defects: a first-principles study, Nanotechnology 20 (2009) 185504.
[17] X. An, J.C. Yu, Y. Wang, Y. Hu, X. Yu, G. Zhang, WO nanorods/graphene nanocomposites for high-efficiency visible-light-driven photocatalysis and NO gas sensing, J. Mater. Chem. 22 (2012) 8525–8531.
[18] J. Dai, J. Yuan, P. Giannozzi, Gas adsorption on graphene doped with B, N, Al, and S: A theoretical study, Appl. Phys. Lett. 95 (2009) 183.
[19] A.V. Markevich, M. Baldoni, J.H. Warner, A.I. Kirkland, E. Besley, Dynamic behavior of single Fe atoms embedded in graphene, J. Phys. Chem. C 120 (2016) 21998–22003.
[20] H. Wang, Q. Wang, Y. Cheng, K. Li, Y. Yao, Q. Zhang, C. Dong, P. Wang,

U. Schwingenschlögl, W. Yang, Doping monolayer graphene with single atom substitutions, Nano Lett. 12 (2012) 141.
[21] A.W. Robertson, B. Montanari, K. He, J. Kim, C.S. Allen, Y.A. Wu, J. Olivier, J. Neethling, N. Harrison, A.I. Kirkland, Dynamics of single Fe atoms in graphene vacancies, Nano Lett. 13 (2013) 1468–1475.
[22] M.A.N. Dewapriya, R.K.N.D. Rajapakse, Effects of free edges and vacancy defects on the mechanical properties of graphene, in: IEEE International Conference on Nanotechnology IEEE International Conference on Nanotechnology, 2014, pp. 908–912.
[23] F. Banhart, J. Kotakoski, A.V. Krasheninnikov, Structural defects in graphene, ACS Nano 5 (2011) 26–41.
[24] E. Ashori, F. Nazari, F. Illas, Influence of NO and (NO)2 adsorption on the properties of Fe-N_4 porphyrin-like graphene sheets, Phys. Chem. Chem. Phys. 19 (2017) 3201.
[25] D. Deng, X. Chen, Y. Liang, W. Xing, Q. Liu, L. Yun, H. Yang, H. Tian, Y. Hu, P. Du, A single iron site confined in a graphene matrix for the catalytic oxidation of benzene at room temperature, Sci. Adv. 1 (2015) e1500462.
[26] Y. Li, Z. Zhou, G. Yu, W. Chen, Z. Chen, CO catalytic oxidation on Iron-embedded graphene: computational quest for low-cost nanocatalysts, J. Phys. Chem. C 114 (2010) 6250–6254.
[27] S. Wannakao, T. Nongnual, P. Khongpracha, T. Maihom, J. Limtrakul, Reaction mechanisms for CO catalytic oxidation by N_2O on Fe-embedded graphene, J. Phys. Chem. C 116 (2012) 16992–16998.
[28] S. Kattel, G. Wang, Reaction pathway for oxygen reduction on FeN_4 embedded graphene, J. Phys. Chem. Lett. 5 (2015) 452–456.
[29] E. Croiset, K.V. Thambimuthu, NOx and SO_2 emissions from O_2/CO_2 recycle coal combustion, Fuel 80 (2001) 2117–2121.
[30] H. Watanabe, J.I. Yamamoto, K. Okazaki, NOx formation and reduction mechanisms in staged O_2/CO_2 combustion, Combust. Flame 158 (2011) 1255–1263.
[31] H. Stadler, D. Ristic, M. Förster, A. Schuster, R. Kneer, G. Scheffknecht, NOx-emissions from flameless coal combustion in air, Ar/O_2 and CO_2/O_2, P. Combust. Inst. 32 (2009) 3131–3138.
[32] T.C. Merkel, H. Lin, X. Wei, R. Baker, Power plant post-combustion carbon dioxide capture: An opportunity for membranes, J. Membrane Sci. 359 (2010) 126–139.
[33] K.H. Tan, T.L. Wang, Asphyxiants: simple and chemical, Ann. Disaster Med. 4 (2005) S35–S40.
[34] S.C. Anenberg, J. Schwartz, D. Shindell, M. Amann, G. Faluvegi, Z. Klimont, G. Janssens-Maenhout, L. Pozzoli, D.R. Van, E. Vignati, Global air quality and health co-benefits of mitigating near-term climate change through methane and black carbon emission controls, Environ. Health Persp. 120 (2012) 831–839.
[35] B.J. Heilman, Photoactive Nitric Oxide Delivery Systems based on Metal Nitrosyl-Biomaterial Composites, Dissertations & Theses – Gradworks, 2015.
[36] M. Hübner, C.E. Simion, A. Tomescu-Stănoiu, S. Pokhrel, N. Bârsan, U. Weimar, Influence of humidity on CO sensing with p-type CuO thick film gas sensors, Sensors Actuat. B Chem. 153 (2011) 347–353.
[37] T. Akamatsu, T. Itoh, N. Izu, W. Shin, NO and NO_2 sensing properties of WO_3 and Co_3O_4 based gas sensors, Sensors-Basel 13 (2013) 12467–12481.
[38] P. Rai, Y.S. Kim, H.M. Song, M.K. Song, Y.T. Yu, The role of gold catalyst on the sensing behavior of ZnO nanorods for CO and NO2 gases, Sens. Actuators, B 165 (2012) 133–142.
[39] D. Cortésarriagada, N. Villegasescobar, A DFT analysis of the adsorption of nitrogen oxides on Fe-doped graphene, and the electric field induced desorption, Appl. Surf. Sci. 420 (2017) 446–455.
[40] G. Kresse, From ultrasoft pseudopotentials to the projector augmented-wave method, Phys. Rev. B: Condens. Matter 59 (1999) 1758–1775.
[41] P. Blochl, E. Blöchl, P.E. Blöchl, Projected augmented-wave method, 1994.
[42] J.P. Perdew, K. Burke, M. Ernzerhof, ERRATA: Generalized gradient approximation made simple, Phys. Rev. Lett. 77 (1996) 3865.
[43] F. Neese, The ORCA program system, Wiley Interdiscipl. Rev. Comput. Molecul. Sci. 2 (2012) 73–78.
[44] P. Lazar, F. Karlický, P. Jurečka, M. Kocman, E. Otyepková, Š.K.M. Otyepka, Adsorption of small organic molecules on graphene, J. Am. Chem. Soc. 135 (2013) 6372.
[45] J. Kysilka, M. Rubeš, L. Grajciar, P. Nachtigall, O. Bludský, Accurate description of argon and water adsorption on surfaces of graphene-based carbon allotropes, J. Phys. Chem. A 115 (2011) 11387.
[46] E. Voloshina, D. Usvyat, M. Schütz, Y. Dedkov, B. Paulus, On the physisorption of water on graphene: a CCSD(T) study, Phys. Chem. Chem. Phys. Pccp 13 (2011) 12041–12047.
[47] I.K. Petrushenko, DFT Study on adiabatic and vertical ionization potentials of graphene sheets, Adv. Mater. Sci. Eng. 2015 (2015).
[48] T. Lu, F. Chen, Multiwfn: A multifunctional wavefunction analyzer, J. Comput. Chem. 33 (2012) 580–592.
[49] U.O. Illinois, Visual molecular, Dynamics (2014).
[50] G. Henkelman, A. Arnaldsson, H. Jónsson, Comput. Mater. Sci. 36 (2006) 354.
[51] Z. Liu, T. He, K. Liu, W. Chen, Y. Tang, Structural, electronic and catalytic performances of single-atom Fe stabilized by divacancy-nitrogen-doped graphene, RSC Adv. 7 (2017) 7920–7928.
[52] Y. Tang, J. Zhou, Z. Shen, W. Chen, C. Li, X. Dai, High catalytic activity for CO oxidation on single Fe atom stabilized in graphene vacancies, RSC Adv. 6 (2016) 93985–93996.
[53] J. Sun, Y.H. Fang, Z.P. Liu, Electrocatalytic oxygen reduction kinetics on Fe-center of nitrogen-doped graphene, Phys. Chem. Chem. Phys. Pccp 16 (2014) 13733–13740.
[54] A. Lee, J. Kang, S. Wei, K.J. Chang, Y. Kim, Carrier-mediated long-range ferromagnetism in electron-doped Fe-C4 and Fe-N4 incorporated graphene, Phys. Rev. B 86 (2012) 165403.
[55] A.V. Krasheninnikov, P.O. Lehtinen, A.S. Foster, P. Pyykkö, R.M. Nieminen, Embedding transition-metal atoms in graphene: structure, bonding, and magnetism, Phys. Rev. Lett. 102 (2009) 126807.
[56] Z.M. Ao, J. Yang, S. Li, Q. Jiang, Enhancement of CO detection in Al doped graphene, Chem. Phys. Lett. 461 (2008) 276–279.
[57] A.S. Rad, E. Abedini, Chemisorption of NO on Pt-decorated graphene as modified nanostructure media: A first principles study, Appl. Surf. Sci. 360 (2016) 1041–1046.
[58] Y. Zou, F. Li, Z.H. Zhu, M.W. Zhao, X.G. Xu, X.Y. Su, An ab initio study on gas sensing properties of graphene and Si-doped graphene, Eur. Phys. J. B 81 (2011) 475–479.
[59] J.H. Enemark, R.D. Feltham, Principles of structure, bonding, and reactivity for metal nitrosyl complexes, Coordin. Chem. Rev. 13 (1974) 339–406.
[60] Y. Tang, W. Chen, C. Li, L. Pan, X. Dai, D. Ma, Adsorption behavior of Co anchored on graphene sheets toward NO, SO_2, NH_3, CO and HCN molecules, Appl. Surf. Sci. 342 (2015) 191–199.
[61] M. Zhou, Y.H. Lu, Y.Q. Cai, C. Zhang, Y.P. Feng, Adsorption of gas molecules on transition metal embedded graphene: a search for high-performance graphene-based catalysts and gas sensors, Nanotechnology 22 (2011) 385502.
[62] M.D. Esrafili, F. Sharifi, P. Nematollahi, Al- or Si-decorated graphene oxide: A favorable metal-free catalyst for the N_2O reduction, Appl. Surf. Sci. 387 (2016) 454–460.
[63] J. Zhao, Z. Chen, Single Mo atom supported on defective boron nitride monolayer as an efficient electrocatalyst for nitrogen fixation: a computational study, J. Am. Chem. Soc. 139 (2017).
[64] G.L. Klimchitskaya, V.M. Mostepanenko, V.M. Petrov, Conductivity of graphene in the framework of Dirac model: Interplay between nonzero mass gap and chemical potential, Phys. Rev. B 96 (2017).
[65] T. Stauber, Plasmonics in Dirac systems: from graphene to topological insulators, J. Phys. Condens. Matter 26 (2014) 123201.
[66] L.G.M. Pettersson, A. Nilsson, A molecular perspective on the d -band model: synergy between experiment and theory, Top. Catal. 57 (2014) 2–13.